Revealing the role of limiting oxygen concentration test for a wick flame in characterizing the liquid fuel flammability

Feng Guo [a*], Nozomu Hashimoto [a], Osamu Fujita [a]

[a] *Division of Mechanical and Space Engineering, Hokkaido University,*

Kita 13, Nishi 8, Kita-ku, Sapporo, Hokkaido, 060-8628, Japan

** Corresponding author: Feng Guo*

TEL: +81 11 706 6387

E-mail address: cumt-guofeng@hotmail.com

Declarations of interest: none.

Abstract

A two-dimensional numerical model was established to simulate the wick combustion system for determining the limiting oxygen concentration (LOC) of organic solvents, called the wick-LOC method. The ethanol wick flame under forced flow with decreased oxygen concentrations in normal gravity was studied numerically. Three simplified reaction mechanisms, 1-step, 2-step, and quasi-global mechanisms of ethanol were employed in the simulations for comparison with experimental results. The responses of flame height and edge flame standoff distance to the oxygen decrease were analyzed for validation. As the oxygen concentration was reduced to the stability limit of the full flame, the blow-off of the edge flame can be observed. By comparing the simulated LOCs and near-limit stabilized flame structures, the 2-step mechanism can reproduce the wick-LOC well, while the quasi-global mechanism can provide a more detailed flame structure. Further investigation into flame blow-off processes revealed that the reaction rate in fuel-lean conditions is more important for determining the wick-LOC, and the local flow velocities at the flame kernel are almost constant until blow-off occurs. By combining the flame stabilization theory with simulations, the physical meaning of the wick-LOC value can be explained as the oxygen concentration where the local flow velocity can be balanced with critical edge flame speed (more fundamentally, the critical laminar burning velocity) in a certain fuel-lean equivalence ratio. Further applications of the wick-LOC method are expected to examine the simplified reaction mechanisms of other liquid fuels.

Keywords

Wick flame, Modeling, Blow-off, Extinction limit, Simplified mechanism, Oxygen limit

1. Introduction

Limiting oxygen concentration (LOC) of a candle-like diffusion flame has been used as a quantitative indicator to evaluate the material flammability. Initiated by the work of Fenimore and co-workers [1], the oxygen index (OI) method has been developed into national and international standards [2,3]. Since the limiting oxygen index (LOI) was confirmed not to be an intrinsic property of the material by a series of investigations [4–7], it has been regarded as a critical condition supporting the downward (opposed flow) flame propagation of a solid specimen [8]. Along with in-depth studies on controlling mechanisms of LOI in terms of radiative, thermal, and kinetic regimes [9–14], many variations from the LOI method have been developed for different application scenarios, such as plastics [15–17], wires [18–20] and fabrics [21–23] for space use, and electrolyte solvents for Li-ion batteries [24–27].

Two extinction branches have been discussed extensively for determining LOC: quenching [11,28,29] and blow-off [30,31]. For the blow-off extinction controlled by the critical Damköhler number, the LOC of a stabilized diffusion flame can be reached when the local flow velocity is comparable to the flame propagation speed at the flame leading edge [32–34], which reveals a potential correlation between the LOC and chemical kinetics. Due to the interaction between the flame and solid surface, not only the combustion reaction in the gas phase but also the finite-rate pyrolysis (gasification) in the solid phase can affect the chemical time for the LOC determination [10,22]. To simplify the complexity of solid combustion, burning liquid fuels through a wick is usually used as a simulant [30,35–37]. However, the effect of the capillarity effect on the burning rate should be noted when the surface saturation is insufficient [35,38].

In our previous work, a wick burner in conjunction with the LOC method was developed to quantify the flammability of electrolyte solvents used in Li-ion batteries, called the wick-LOC method [24–26]. Under well-specified experimental conditions, the surface saturation of the wick can be maintained to provide a constant burning rate during combustion. By precisely adjusting the oxygen concentration under constant external flow velocity, we expected that the wick-LOC can correlate to the combustion reaction kinetics of gasified fuel more directly, especially for the LOC of full flame (envelope flame covering the whole wick) [26,27]. Therefore, numerical approaches using Computational Fluid Dynamics (CFD) tools are necessary to model the wick burner

for more insights into the meaning of the wick-LOC in characterizing the liquid fuel flammability.

Take a glance at the relevant modeling studies of candle flames, LOI, and cup burner tests, their development and notable points are valuable for reference. Kosdon et al. [39] studied the standoff distance of the envelope flame over vertical cellulosic cylinders using a similarity theory. Chen and coworkers [37,40] established numerical models for buoyant ethanol-air wick flame and its oscillations. Meanwhile, Riley [41] has adopted a flame-sheet model for the candle. However, the above early works assumed a one-step infinitely fast reaction for the gas phase combustion, which is not able to discuss the extinction phenomena. Since 2000, Dietrich [42] employed one-step finite-rate kinetics for the candle flame in a non-buoyant atmosphere and predicted the pre-extinction flame oscillation in a decreased ambient oxygen. Further, Tien and coworkers modeled the gravity effect on saturated candle flames under a constant boundary condition [43], and self-trimmed candle flames under a coupled model of gas phase and porous media flow [38]. In addition to modeling of candle wick flames, Kumar, Tien and co-workers [44–47] have built more detailed models of LOI tests for other solid slabs, numerically predicting the flame behaviors to oxygen and flow changes, although they have not focused on chemistry.

In this study, a two-dimensional (2D) numerical model was established for the wick-LOC test. Ethanol (EtOH) was used as a reference fuel with different simplified reaction mechanisms. We investigated the wick flame behaviors under decreased oxygen concentration with the comparison between experiments and simulations. The stabilization (or extinction) at the flame leading edge was analyzed under the wick-LOC configuration for a detailed understanding.

2. Experimental methods

The experimental setup of the wick-LOC method is identical with our previous works [24–27]. It consists of the candle-wick burner, the gas supply system, the fueling system, and measuring devices, as shown in Fig. 1. In this work, the cotton wick (6 mm in length and 5 mm in diameter) soaked with ethanol generates a wick flame. The fueling system maintains the liquid level to keep saturation of the wick during combustion, which facilitates the simplification of solid-phase models in numerical simulations. The gas supply system provides N_2/O_2 mixed gas with a constant flow rate (0.1 m/s) to the chamber. The wick-LOC value can be determined

by adjusting the oxygen concentration of the external flow step-by-step. The flame behaviors were recorded by video camera to compare with the numerical results. The wick surface temperature was measured using a fine thermocouple (wire diameter 0.1 mm) as specified in our previous work [27].

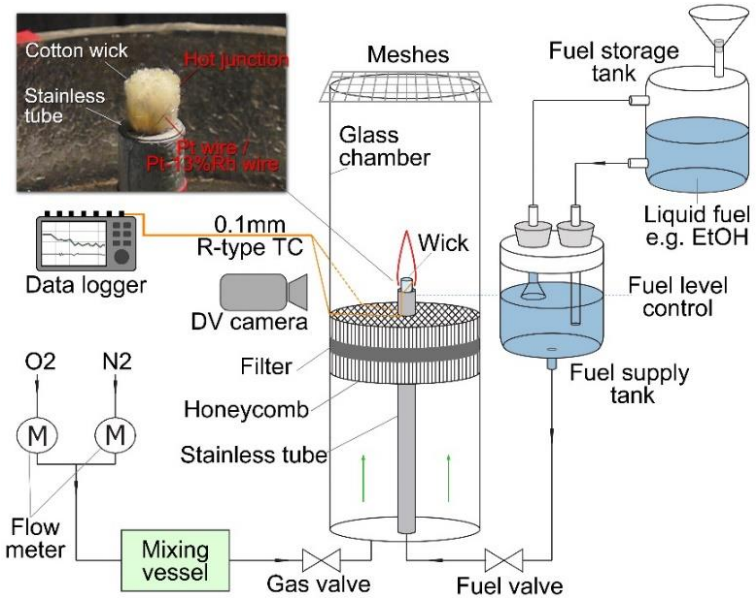

Fig. 1. Experimental setup schematic of the wick-LOC method [24–27].

As discussed in the previous work [26], two types of wick flames can be observed during oxygen decrease, an envelope flame covering the side of the wick called full flame, and a small flame downstream of the wick called wake flame. According to the surface temperature measurement of the wick, this work will focus on the wick-LOC of full flame (full flame stability limit) for the judgment of flame extinction in numerical simulation. As shown in Fig. 2, eight points were selected for the surface temperature measurements, and the time-averaged temperatures of these points at different oxygen levels were plotted in Fig. 2 (b) and (c). The measured wick surface temperature of each point is close to the boiling point of ethanol ($B.P._{EtOH}$ = 78 ℃) under the full flame conditions, while it has a considerable fluctuation (20~40 ℃) during near-limit oscillating flame, as discussed in the previous experimental study [27]. If we limit the scenario to the flame behaviors until the full flame limit occurs, the surface temperature of the wick can be assumed as a constant value (*B.P.* of the fuel). Unlike the ordinary candle wick, the surface temperature does not fully reflect the saturation concentration in the present wick-LOC apparatus. The special design of the fueling system can stabilize the liquid level during the experiments, which can ensure the ethanol saturation on the 6 mm long wick without self-trimming. This has

been verified by changing the wick length in our previous work [24]. Therefore, the boundary condition of the wick surface can be simplified to the constant temperature in a saturated state when establishing the numerical model, and the simulated flame behavior until the full flame limit can also be reliable enough. Similar treatments are also adopted in previous numerical studies on candle-like flames [42,43,47].

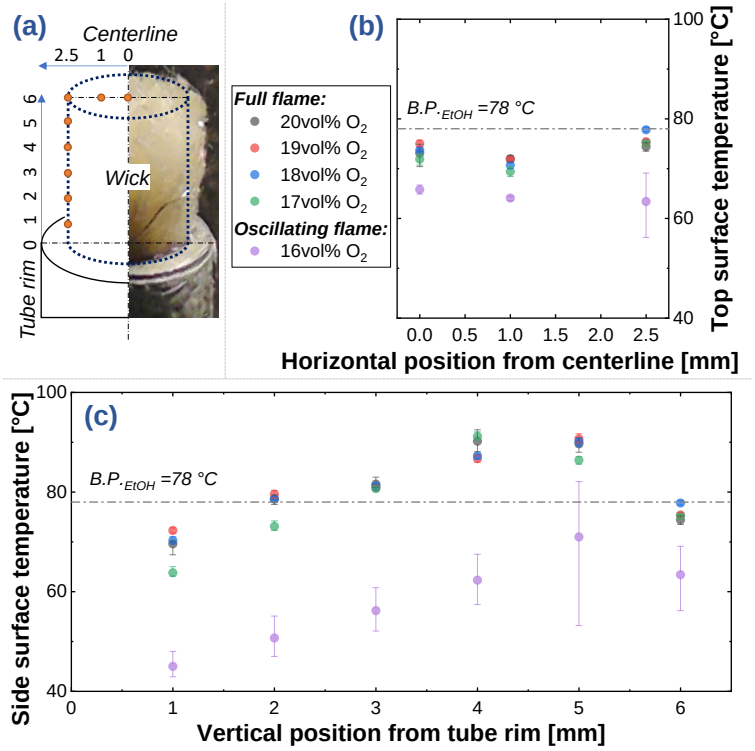

Fig. 2. Surface temperature measurement of the ethanol wick during combustion at different oxygen levels. (a) measurement points; (b) top surface temperature; (c) side surface temperature.

3. Numerical simulation

3.1 Governing equations

The 2D numerical model of the wick burner was established utilizing FrontFlow/Red (NuFD/FFR) [48], a multi-scale and multi-physics CFD solver initially developed at the Institute of Industrial Science (IIS), The University of Tokyo, Japan as a part of the project Frontier Simulation Software for Industrial Science [48]. Along with low Mach number approximation for the compressible flow under a normal gravity environment, the conservation equations of mass, momentum, energy, and chemical species are directly solved for the gaseous phase, as well as the equation of state:

Mass conservation:

$$\frac{\partial \rho}{\partial t} + \frac{\partial}{\partial x_j}(\rho u_j) = 0 \tag{1}$$

Momentum conservation:

$$\frac{\partial \rho u_i}{\partial t} + \frac{\partial}{\partial x_j}(\rho u_i u_j) = -\frac{\partial p}{\partial x_i} + \frac{\partial}{\partial x_j}\left\{\mu\left(\frac{\partial u_i}{\partial x_j} + \frac{\partial u_j}{\partial x_i} - \frac{2}{3}\delta_{ij}\frac{\partial u_k}{\partial x_k}\right)\right\} + \rho g_i \tag{2}$$

Energy conservation:

$$\frac{\partial \rho h}{\partial t} + \frac{\partial}{\partial x_j}(\rho h u_j) = -\frac{\partial p}{\partial t} + u_j\frac{\partial p}{\partial x_j} + \mu\left(\frac{\partial u_i}{\partial x_j} + \frac{\partial u_j}{\partial x_i}\right)\frac{\partial u_i}{\partial x_j} + \frac{\partial}{\partial x_j}\left(\lambda\frac{\partial T}{\partial x_j}\right) + \frac{\partial}{\partial x_j}\left(\rho\sum_s h_s D_s\frac{\partial Y_s}{\partial x_j}\right) + Q \tag{3}$$

Species conservation:

$$\frac{\partial \rho Y_s}{\partial t} + \frac{\partial}{\partial x_j}(\rho Y_s u_j) = \frac{\partial}{\partial x_j}\left(\rho D_s\frac{\partial Y_s}{\partial x_j}\right) + \omega_s \tag{4}$$

Equation of state:

$$p = \rho RT\sum_s \frac{Y_s}{M_s} \tag{5}$$

where ρ is density; u_j is velocity in the x_j direction; p is dynamic pressure; δ_{ij} is the Kronecker delta; g is the gravitational acceleration (-9.8 m/s^2 in this work); h is the mass-weighted enthalpy of the gas mixture; μ is the dynamic viscosity; λ is thermal conductivity of the gas mixture; T is temperature; D_s is diffusion coefficient of species s, Y_s is the mass fraction of species s; Q is the source term; ω_s is the volumetric mass production rate of species s; R is the universal gas constant, and M_s is the molecular weight of species s.

The governing equations for reacting flows are discretized using the finite volume method (FVM) on the structured grid cells as described in the next section. The discrete ordinates method (DOM) was employed to solve the radiative heat transfer with the gray gas model. By preliminary estimation of the Reynolds number (Re ~ 500), the Direct Numerical Simulation (DNS) was performed without considering the turbulent model. The convective terms for momentum, enthalpy, and mass fractions were approximated by a second-order central difference scheme. Time integration was performed using the Euler implicit scheme with a constant time step.

The temperature dependent viscosity was solved by Sutherland's formula:

$$\mu = \mu_0\left(\frac{T_0 + C}{T + C}\right)\left(\frac{T}{T_0}\right)^{3/2} \tag{6}$$

where the reference viscosity of air μ_0 = 1.18172$\times 10^{-5}$ Pa·s, at reference temperature T_0 = 293.15 K, and Sutherland constant C = 117 K.

The simplified transport model referring to Smooke [49] was employed in the present simulation model, where the ratio of the thermal conductivity (λ) to the specific heat at constant pressure (c_p) is expressed as a function of temperature.

$$\frac{\lambda}{c_p} = A\left(\frac{T}{T_0}\right)^{\gamma} \tag{7}$$

where coefficients A = 2.581×10-5 kg/m/s and γ = 0.7, T_0 = 298 K as the reference temperature. Since the μ is solved by Sutherland's formula, the thermal conductivity (λ) and mass diffusivity (D) can be solved by specifying Prandtl (Pr) and Schmidt (Sc) numbers, respectively.

$$\lambda = \frac{c_p \mu}{Pr} \tag{8}$$

$$D = \frac{\mu}{\rho Sc} \tag{9}$$

For simplification, the Prandtl and Schmidt number have been set to Pr = Sc = 1. It should be noted that the Lewis number is thus be set to unity to avoid the impact of differential diffusion interfering with the discussion of the role of chemical reactions. After establishing the relationship between the wick-LOC and the key reaction parameters, the discussion of the differential diffusion will be the next step of our future work.

3.2 Computation domain and boundary conditions

The numerical model was applied to an axisymmetric 2D mesh with a shortcake shape. The schematic of the computational domain with dimension information is shown in Fig. 3 (a). The non-uniformed rectangular meshes were densified around the wick region. As illustrated in Fig. 3 (a), a high-temperature area with a stoichiometric EtOH-air mixture was set as the initial condition for a successful ignition at the beginning, while the other region was set at room temperature with 20% oxygen. 10 boundaries were set in the model. Symmetrical boundaries were set for the two faces in y-direction. The outside wall follows the logarithmic law, while the centerline is a free-slip boundary. The inlet boundary supplies N_2/O_2 mixed gas with 0.1 m/s at room temperature (300 K). The outlet boundary is at atmospheric condition allowing the mass transfer. The temperature of the wick surface was set as 351 K (boiling point of ethanol) all the time, which has been validated experimentally as a proper value for the full flame scenario as explained in Section 2. The gas mole fraction of

ethanol at wick surfaces was set as 1.0 by assuming the saturated state at the boiling point, which can simplify the evaporation model.

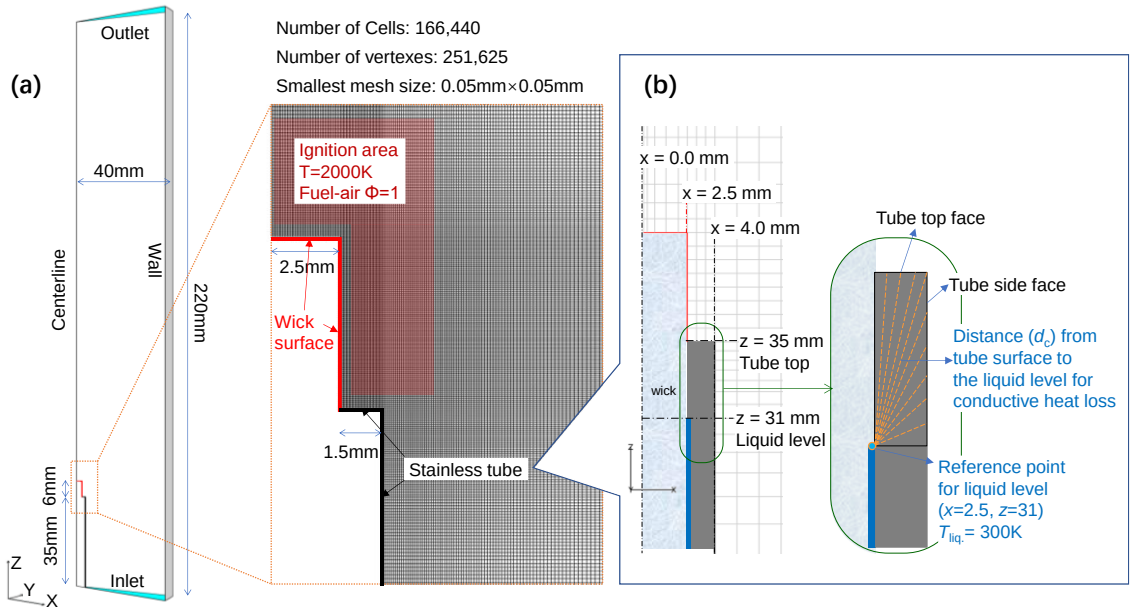

Fig. 3. Schematic of the 2-D computational domain.

The thermal boundary condition of the tube rim can affect the stability of the flame edge, especially when we compare adiabatic and non-adiabatic boundaries. If an adiabatic boundary was set for the tube rim, the flame edge can attach to the tube rim and the LOC of the flame could be lower (more stable). Therefore, it is necessary to set a thermal resistance for the tube rim and give a considerable heat loss to reproduce the standoff distance of the flame edge. The treatment of boundary conditions for the stainless tube surfaces allows heat loss from the gas-phase cell to the surface. The top and side faces of the tube are wall type boundary without mass transfer, the emissivity of the surface was set as 0.8. As shown in Fig. 3 (b), we set the virtual reference point to represent the liquid level in the wick-LOC experiments. The reference temperature ($T_{liq.}$) keeps constant as 300 K for the position at $0 \leq z \leq 31$ mm and x = 2.5 mm. The initial temperature of the tube boundaries is 300 K. The thermal conductivity of the stainless tube is 14.9 W/m·K referring to the database [50]. The heat flux from the tube surface is expressed as $q_w = h\ (T_w - T)$, where T_w is the wall temperature and T is adjacent gas temperature. Referring to the boundary condition treatment of the burner wall in the previous work [51,52], the h is nominal heat transfer coefficient to consider the thermal resistance of the stainless tube, expressed as $h = 14.9 / (d_c/1000)$,

where d_c is the distance for the surface to the reference point, the unit is mm for convenience. For $0 \leq z \leq 31$ mm, $d_c = 1.5$ mm, same to the tube wall thickness; while for 31 mm $< z \leq 35$ mm, $d_c^2 = (x - 2.5)^2 + (z - 31)^2$, as indicated by the dashed lines in Fig.3 (b) with orange color. With above setting, the relatively low temperatures at the tube rim also indicate a sufficient heat loss from the flame edge to the tube rim, as shown in the supplementary materials (S.1).

3.3 Chemical reaction models for combustion

In the simulation, ethanol is the sole gaseous fuel and diffuses to the co-flow of the O_2/N_2 mixture. Three simplified reaction mechanisms of ethanol combustion, single-step (WD-1S), two-step (WD-2S), and quasi-global (WD-QG) mechanisms, were employed according to Westbrook and Dryer [53]. The reaction parameters are listed in Table S2.1 of the supplementary materials (S.2). Units are cm-sec-mole-kcal-Kelvins. The reaction rate is expressed by

$$\omega = AT^n exp\left(-\frac{E}{RT}\right)\prod_s [X_s]^{Cs} \tag{7}$$

where A is pre-exponential factor; E is activation energy; and $[X_s]$ is the molar concentration of species s. The superscript C_s is the order of the reactant, corresponding to a, b, and c listed in Table S2.1; and n is the temperature component. The chemical source term in Eq. (4) is obtained by $\omega_s = \nu_s M_s \omega$ where ν_s is the stoichiometric coefficient of species s. The WD-QG mechanism consists of an global reaction of fuel oxidation and 21 elementary reactions of the CO-H_2-O_2 system [53], where reverse rates of elementary reactions were computed from relevant equilibrium constants. The thermodynamic properties of the species are obtained from the CHEMKIN database [54]. For the simulations employing different reaction mechanisms, different sizes of time step (Δt) were used, $\Delta t = 10^{-5}$ s for WD-1S and WD-2S, and $\Delta t = 10^{-6}$ s for WD-QG. The grid and time step dependencies were all analyzed considering the balance of accuracy and computational cost, as shown in the supplementary materials (S.3).

4. Results and discussion

4.1 Stabilized flame behaviors

The flame behaviors in decreased oxygen concentration were observed by experiments and numerical

simulations. As simplified mechanisms (WD-1S and WD-2S) were employed in simulations, the fractions of radicals and soot are not available. Thus, we used simulated reaction rate contours which can provide a clear flame shape to accurately compare with the experimental flame images capture by DV camera. As shown in Fig. 4, the flame height change was compared between direct images of ethanol flame and simulated ethanol consumption rate by WD-1S, which are quite similar. From the center to the sides, the heights of both flames slightly increase with the decrement in oxygen level. The flame leading edges were slightly lifted from the supporting tube. The edge flames have bi-brachial or tri-brachial flame structures with a small rich premixed flame (RPF), similar to the description from Ref. [32].

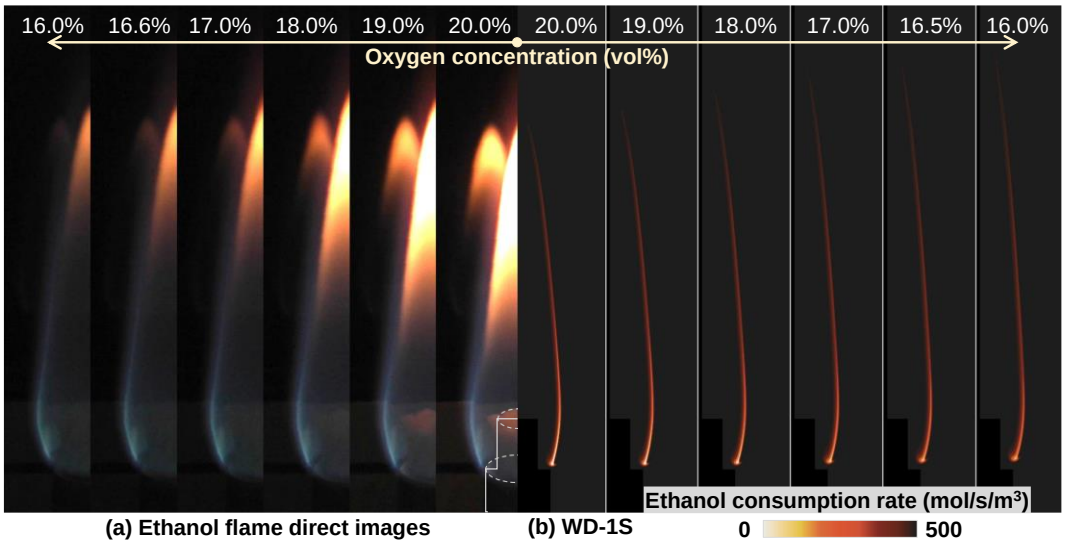

Fig. 4. Comparison of axisymmetric ethanol wick flames at different oxygen levels between (a) experimental images and (b) simulated distribution of ethanol consumption rate employing WD-1S. The background flame tips of the experimental images are the reflections of the glass chamber.

Different from WD-1S, the 2-step mechanism (WD-2S) includes the oxidation of CO and dissociation of CO_2, which can provide additional information about the flame under decreased oxygen concentration. Figure 5 compares the ethanol consumption rate and CO_2 production rate at different oxygen levels. Similar to experiments, the flame height increases with oxygen decrease. From the CO_2 production rate images by WD-2S, the inner layer of the flame sheet has a negative value of CO_2 production due to the high flame temperature. As the oxygen decreases, the dissociation of CO_2 becomes weaker because of lower flame temperature.

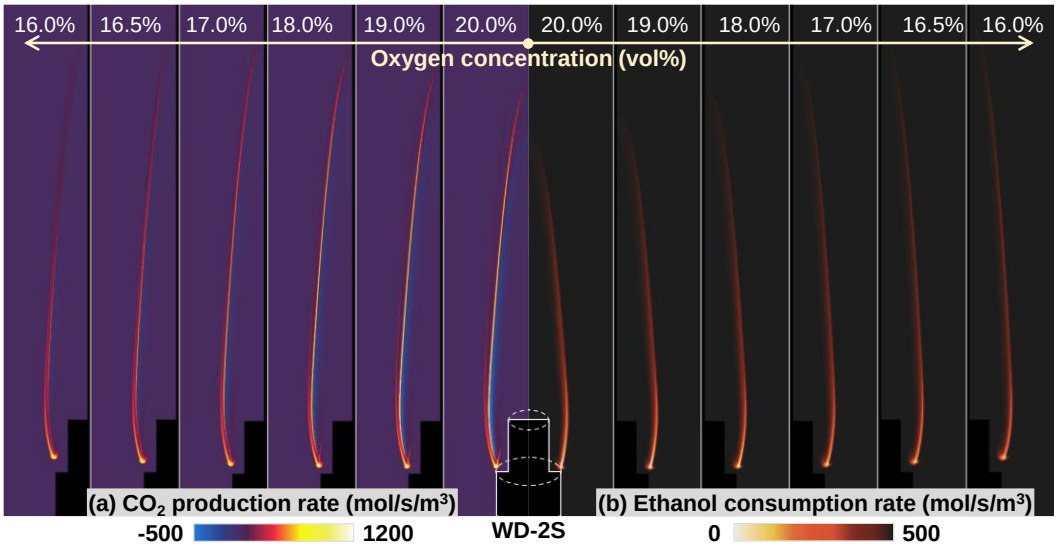

Fig. 5. Simulated distributions of (a) CO_2 production rate and (b) ethanol consumption rate of the wick flame at different oxygen levels, employing WD-2S.

As WD-QG includes one global reaction of ethanol oxidation and 21 steps of detailed mechanism for CO-H_2-O_2 reactions, more detailed information of the wick flame can be provided, like the evolution of some important radicals (OH* and H*). Figure 6 shows the distributions of the reaction rates and radical mole fractions from the simulations employing WD-QG. The flame height varying with the oxygen decrease is almost consistent with the tendency in experiments, but the LOC from WD-QG is higher than the others. At the stability limit (around 16.6%) of the full flame from WD-QG, the flame leading edge was lifted and re-stabilized at the wake region, and the ethanol consumption rate of which shows an asymmetric tri-brachial structure. However, due to the simplification of wick boundaries in this work, we will focus on the onset of the full flame limit rather than the stabilized wake flame. Figures 6 (c) and (d) show the distributions of OH and H radicals, which are generally used to characterize the flame sheet. The similar distributions of H* and reaction rates confirmed that it is reasonable using ethanol consumption rate to characterize the flame height in comparison with the experiments. More distributions of temperature, velocity, and other species by the three mechanisms can be found in the supplementary materials (S.4).

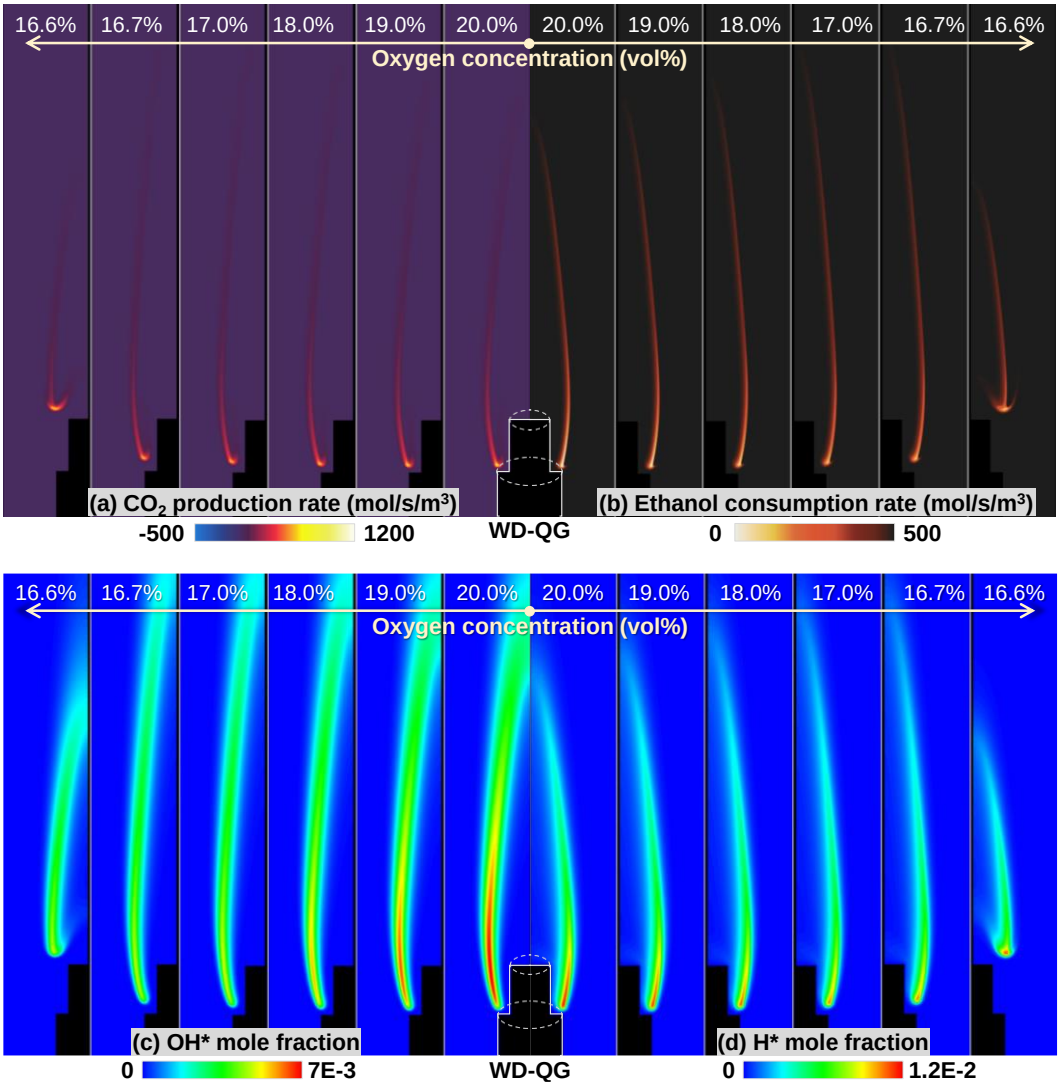

Fig. 6. Simulated distributions of (a) CO_2 production rate, (b) ethanol consumption rate, (c) OH* mole fraction, and (d) H* mole fraction of the wick flame at different oxygen levels, employing WD-QG.

4.2 Flame heights and standoff distances

To further validate the numerical model of the wick flame, the flame heights (H_f) and standoff distances (D_z) are compared between experiments and simulations, as shown in Fig. 7 and Fig. 8, respectively. As there is no soot formation model in the numerical simulation, the determinations of flame height (H_f) from the flame tips to the stainless tube rim are different for experiments and simulations. The experimental H_f was determined by the visible flame luminance [27]; while the numerical H_f was determined by the stoichiometric mixture fraction value [55]. Because the luminous flame height is controlled by the soot concentration and flame temperature, it always has a 10% uncertainty (generally 10% higher) when compared to the stoichiometric flame height [56]. When the soot is getting less during oxygen decrease, the luminous flame height could be closer to

the stoichiometric flame height. Therefore, the flame heights given by different kinetic models have a reasonable prediction according to the qualitative comparison. On the other hand, D_z is defined as the vertical distance from the rim of the supporting tube to the flame edge, which is determined by the maximum luminance in experiments and the maximum reaction rate in simulations, respectively. For both experiments and simulations, the standoff distance slightly increased with oxygen decreases from 20% to the LOCs, where the experimental and simulation results by WD-2S have a good agreement. As the standoff distance increases, the conductive heat loss from the flame edge to the stainless tube rim reduces. Thus, the flame can be stabilized at different vertical positions. When the oxygen is approaching the LOCs, the standoff distances of experimental and simulated flames are all around 1.7 mm. With further decrement of oxygen, the flames are detached from the wick side, as indicated by the vertical lines in Fig. 8. The shadowed areas in Fig.7 and Fig. 8 indicate the different LOCs given by three mechanisms. Near the LOC of the full flame, the edge flame is in the critical condition of stabilization. For the edge flame structures near LOCs by simulation, the radial profiles of the structure near the flame kernel (with the highest reaction rate [57]) can be found in the supplementary materials (S.5), where the WD-QG can provide more detailed information.

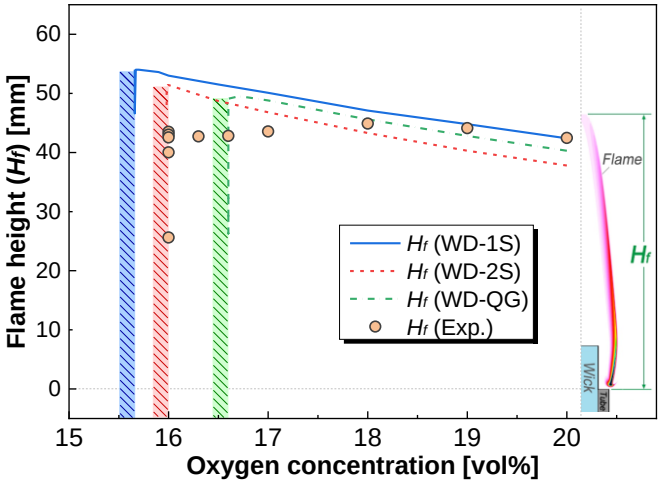

Fig. 7. Flame heights at different oxygen levels from experiments and simulations.

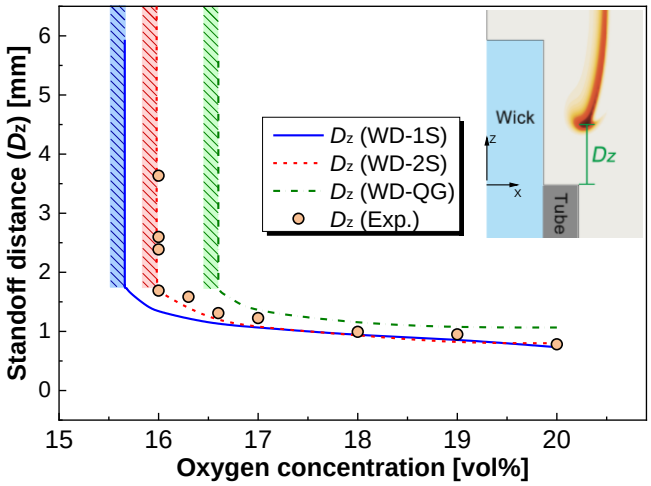

Fig. 8. Standoff distances of flame edges at different oxygen levels from experiments and simulations.

4.3 Flame blow-off extinction

The full flame was validated by examining the flame lengths and the standoff distances of the flame edge, which implied a reasonable boundary condition of the model for the steady state of the full flame. However, under the simplification of the constant thermal boundary of the wick surface, a potential wake-stabilized flame observed in the previous experimental works [24,26] may not be exactly reproducible, because the cooling wick surface in the actual wake-stabilized flame could cause a larger heat loss from the flame edge. Nevertheless, the full flame blow-off due to the reduced oxygen concentration is an instantaneous process (< 0.1 s from the bottom to the top of the wick [27]), and the temperature of the wick surface that loses flame coverage has a negligible effect on this process. Therefore, the destabilization of the full flame at the limit conditions in the present model can provide useful information for our understanding of this near-limit flame behavior.

By decreasing the oxygen concentration at the constant external flow velocity, flame blow-off extinction can be observed when the oxygen level reaches the LOC of the full flame. So, we can clarify how the flame edge moves downstream when it is destabilized. Figures 9 presents the contours of volumetric heat release rate (*HRR*), temperature (*T*), oxygen mole fraction (X_{O2}), and equivalence ratio (Φ) around the flame leading edge for the simulations employing WD-2S. In Fig.9, the calculated LOC of the ethanol full flame predicted by WD-2S is between 15.98% and 16.0%, which is very close to the experimental LOC at 16.0±0.1%. The HRR image shows a triple-flame structure at the flame leading edge, the darkest part reveals the flame kernel with the highest reaction rate. The temperature contours (red lines) indicate that the highest temperature region exists

downstream of the flame kernel. There is a gradient of Φ at the flame leading edge from the rich side to the lean side, where $\Phi < 1$ at the flame kernel. When the oxygen was reduced to 15.98% from 16.0%, the flame kernel retreated downstream through the line of $0.5<\Phi<1.0$. It implied that the reaction in fuel-lean conditions could be more important for the blowoff of the wick-LOC configuration. Similar blow-off extinction processes of full flames can be found in the supplementary materials (S.6) but under a lower LOC given by WD-1S and a higher LOC given by WD-QG than the experiments.

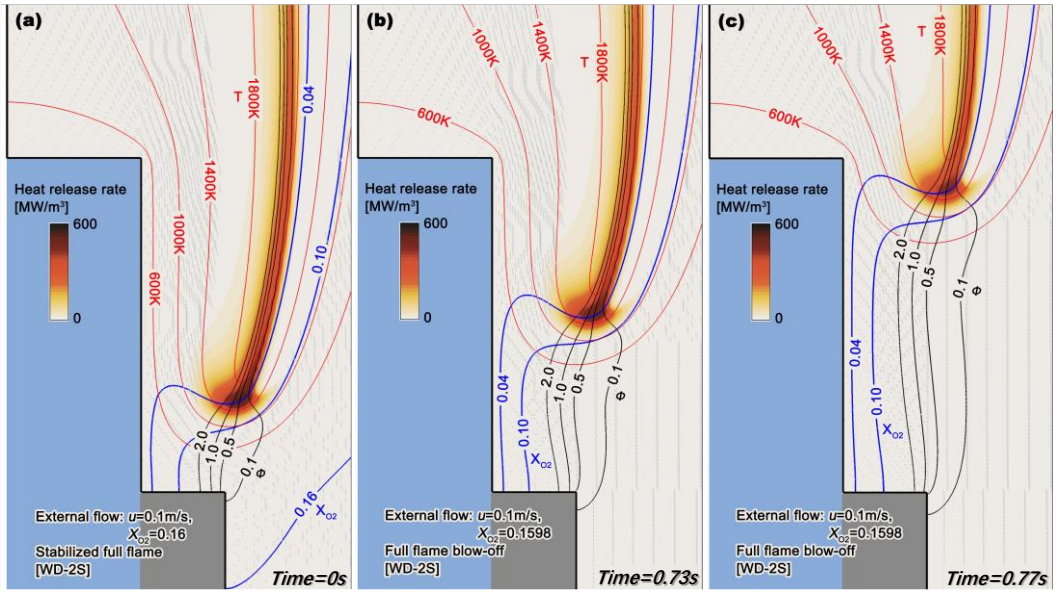

Fig. 9. Time evolutions of heat release rate distributions, temperature, oxygen mole fraction and equivalent ratio contours near the wick flame base at LOC. (a) stabilized full flame at X_{O2}=16.0%, (b) and (c) full flame blow-off sequence at X_{O2}=15.98%, from simulations employing WD-2S.

4.4 Local flow velocities and edge flame speeds

Before going further into the stabilization mechanism of the full wick flame, it is necessary to briefly discuss the similarities and differences between the full wick flame and the conventional jet diffusion flame. In principle, the stabilization mechanism is the same, which is controlled by the Damköhler number under the balance of the chemical time of the flame edge and the residence time of the local flow [32]. However, the typical configurations are quite different. In general, the stability of the jet diffusion flame mainly depends on the fuel jet velocity, which is much higher than the oxidizer co-flow. Therefore, most of the jet diffusion flame has a large inward rich premixed flame wing [58], and the flame kernel is usually located in the rich premixed

branch [58–60]. The blowoff limits of a jet diffusion flame have always been determined by decreasing the residence time (increasing the jet flow velocity). In contrast, for the full wick flame in this work, the fuel was supplied by diffusion at a very low velocity compared to co-flow. The residence time (or local flow velocity) is mainly controlled by the constant oxidizer co-flow and the buoyancy induced flow, which has a very limited variation before the stability limits. The full wick flame kernel was stabilized in the lean premixed branch and its blowoff limit was determined by increasing the chemical time at the flame edge (reducing the oxygen concentration).

By reproducing the flame blowoff for the wick-LOC configuration with simulations, it is possible to clarify the flame propagation speed and local flow velocity at the flame leading edge especially at the stability limits of full flames. Utilizing numerical simulations, the local flow velocity (U_r) at the flame leading edge can be determined under different oxygen levels, which is almost impossible via the experimental approach. As shown in Fig. 10, the symbols represent the U_r at the position of the flame kernel measured from the simulations employing three different reaction mechanisms. For the simulation results employing WD-1S and WD-2S with decreasing oxygen concentrations, the U_r values of stabilized full flame are almost constant at around 0.3 m/s, while it is around 0.32 m/s in the case of WD-QG. There are sudden increases in U_r at lower oxygen levels, which indicate the stability limits of full flames ($LOC_{Sim.}$), although they have different discrepancies from the experimental LOC (gray barriers labeled as $LOC_{Exp.}$ in Fig. 10). As the designed external flow velocity is 0.1 m/s, the buoyancy-induced flow contributes about 0.2~0.22 m/s to the local flow velocity at the flame kernel for the stabilized full flames.

On the other hand, the edge flame speed (S_e) should decrease with the oxygen reduction and become comparable with the U_r. By reviewing the correlations of S_e [32], the maximum edge flame propagation speed ($S_{e,max}$) is proportional to the stoichiometric laminar burning velocity ($S_{L,st}$) for the symmetrical triple flame in a 2-D mixing layer [61,62]:

$$\frac{S_{\mathrm{e,max}}}{S_{\mathrm{L,st}}} \cong \left(\frac{\rho_{\mathrm{u}}}{\rho_{\mathrm{b,st}}}\right)^{1/2} \tag{8}$$

where ρ is the density and the subscripts u and b indicate unburned and burnt, respectively. By substituting the $S_{L,st}$ calculated by Chemkin Pro into Eq. (8) employing the corresponding reaction mechanisms, we can estimate

the $S_{e,max}$ for ethanol at different oxygen concentrations, as plotted by the dashed lines (labeled as Φ = 1.0) in Fig. 10. The $S_{e,max}$ dramatically declined with oxygen decreases, but it is still larger than the U_r at the $LOC_{Sim.}$, which means, the $S_{e,max}$ estimated by the $S_{L,st}$ cannot reflect the critical condition for the instability of full flame on the wick flame configuration. According to the observation of flame blow-off in the last section (Fig. 9), the flame leading edge retreated along the fuel-lean streamlines. The edge flame propagation speed (S_e) should correspond to the laminar burning velocity with a certain equivalence ratio ($S_{L,\Phi}$) at the flame kernel, which can be expressed as:

$$S_e \cong S_{L,\Phi}\left(\frac{\rho_u}{\rho_{b,\Phi}}\right)^{1/2} \tag{9}$$

where $\rho_{b,\Phi}$ is the burnt gas density at an certain equivalence ratio. The changes of S_e with oxygen concentration at different Φ were plotted as lines in Fig. 10. The differences between the S_e and U_r at higher oxygen levels are attributed to the heat loss of the flame edge, mainly by the conductive heat from the flame edge to the supporting tube. Then, we can find the specific Φ where the S_e is comparable to the U_r at the $LOC_{Sim.}$ given by different reaction mechanisms, as shown by the solid lines in Fig. 10 (a)~(c). Therefore, the physical meaning of the wick-LOC value can be explained as the oxygen concentration where the local flow velocity can be balanced with critical edge flame speed (more fundamentally, the critical S_L) at a certain fuel-lean equivalence ratio. Here, the Φ = 0.8 for WD-1S and WD-2S, and Φ = 0.76 for WD-QG. Note that this certain Φ iso-contour is given by the simplification of the unity Lewis number. Since the differential diffusion always affects the thermal-diffusive stability of the flame, the non-unity Lewis number may cause slight shift of this particular Φ iso-contour. The specific Φ value relies on the model simplification, but the trend for a certain fuel-lean condition for the correction of the Eq. (8) should be the same. Future work will be performed to investigate the sensitivity of the potential factors.

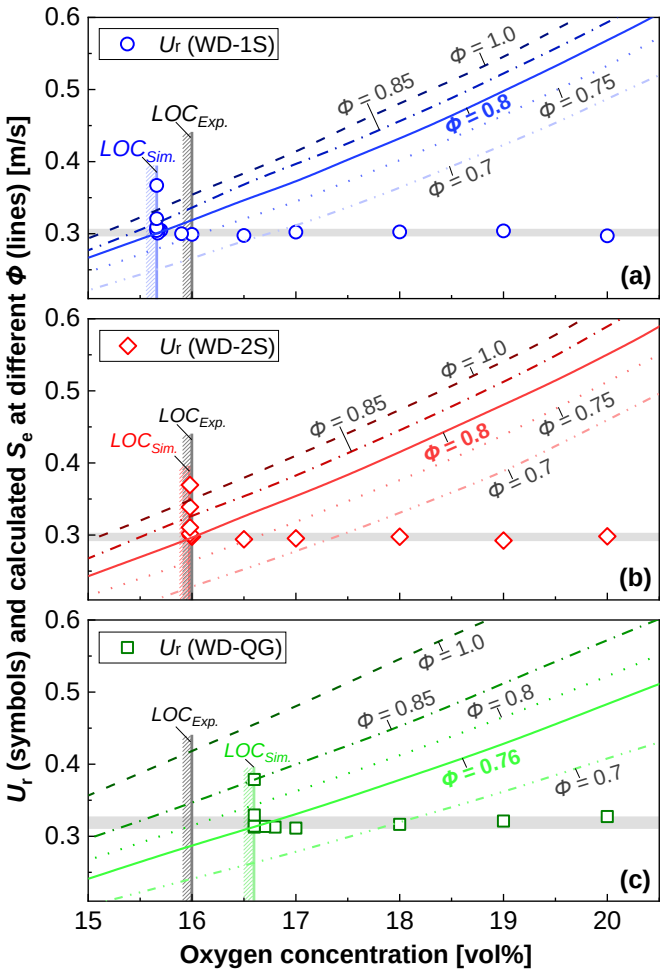

Fig. 10. Comparison of calculated ethanol edge flame propagation speeds (S_e) and local flow velocities (U_r) at different equivalence ratios (Φ) as the change of oxygen concentration from simulations employing (a) WD-1S, (b) WD-2S and (c) WD-QG. Symbols represent the U_r extracted from the simulation results; lines represent the S_e at different Φ; barriers are LOC values.

By using the well-known simplified chemical kinetic models with different complexity, the results showed that the edge flame stabilization mechanism is applicable to the wick flame. In addition, the certain equivalence ratio for the flame stabilization of the wick flame is not so sensitive to the complexity of the chemical model. Since we have a clear correspondence between the wick-LOC value and S_L by above discussions, we can expect to use the experimental wick-LOC to examine the accuracy of reaction mechanism employed in the simulations. Here, the $LOC_{Sim.}$ from WD-2S (15.99%±0.01%) has a very good agreement with the $LOC_{Exp.}$ (16.0%±0.1%), so we can confirm whether the calculated S_L by WD-2S at $\Phi < 1$ is consistent to the experimental S_L. We compared the S_L curves of ethanol-air premixed flames among calculations and experiments from the various references, as shown in Fig. 11. The laminar flame speed calculations were performed using mixture-averaged

transport model. There are considerable discrepancies between simplified mechanisms [53] and detailed mechanisms [63,64] in the stoichiometric condition, but the S_L of WD-1S and WD-2S at $\Phi \leq 0.8$ is similar to the experimental results [65–68]. It shows that the WD-2S can predict better than other mechanisms for both the wick-LOC and the S_L at $\Phi \leq 0.8$. In addition, the order of the S_L curves by WD-1S, WD-2S, and WD-QG in the range of $0.5<\Phi<0.8$ are consistent with the order of reactivity in terms of simulated LOC. Therefore, in addition to the flammability evaluation, the combination of wick-LOC experiments and numerical simulations could be a potential benchmark test for a simplified combustion mechanism in a lean condition. Reversely, we can possibly estimate or optimize the simplified reaction parameters of other liquid combustibles by numerically reproducing the wick-LOC experiments. It also inspired us that the simplified chemistry of liquid fuel could be optimized by adjusting the pre-exponential factors of the first-step reaction to give a better prediction of S_L in the fuel-lean condition. Further exploration will be performed in the future by application into more liquid combustibles including formulated electrolyte solvents and organic fuels with the consideration of differential diffusion effect in the transport model.

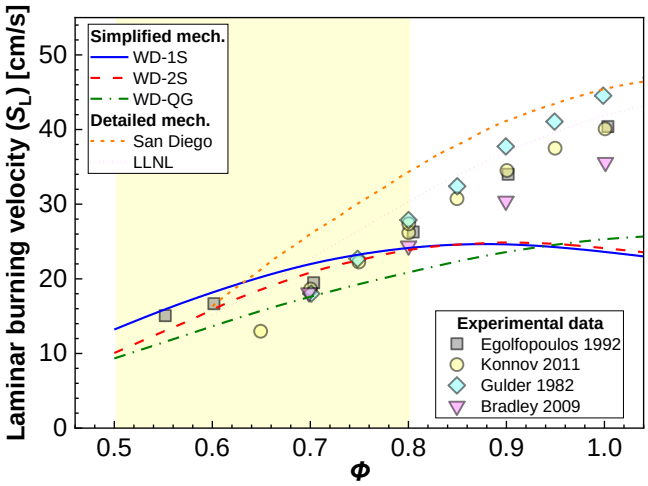

Fig. 11. Laminar burning velocity (S_L) comparison among calculations (employing different reaction mechanisms [53,63,64]) and experiments [65–68] of ethanol-air mixture under atmospheric pressure and room temperature.

5. Conclusions

To reveal the role of wick-LOC method in characterizing the flammability of liquid fuel, a series of numerical studies have been conducted for an ethanol wick flame under decreased oxygen concentration

employing three simplified reaction mechanisms, WD-1S, WD-2S, and WD-QG. The numerical results of LOC, flame height and edge flame standoff distance have been compared with the wick-LOC experiments showing reasonable agreements, which indicate that the reduced kinetics are sufficient for the wick-LOC modeling. The stabilized flame structure at the flame leading edge has been investigated near the LOC condition, which indicates the mismatching between the HRR peaks and the stoichiometric line. Further analysis of flame blow-off processes revealed the importance of reaction rate in the fuel-lean condition. By applying the flame stabilization theory to the wick flame configuration, there was an almost constant local flow velocity at the wick flame leading edge until the full flame blow-off occurred, and the estimated edge flame speed at a certain fuel-lean condition ($\Phi \leq 0.8$ in this work) is comparable with the local flow velocity near the LOC condition. Although the specific equivalence ratio may be different due to simplifications in the numerical model, the basic conclusion is the same that the LOC is mainly controlled by the edge flame propagation speed at a certain fuel-lean condition.

The wick-LOC works as the oxygen concentration where the local flow velocity can be balanced with critical S_L at a certain fuel-lean equivalence ratio, which is expected to examine the simplified reaction mechanisms of other liquid combustibles. Further study on different fuel types will be conducted with optimized boundary conditions and more detailed reaction mechanisms, in the future.

Acknowledgements

This work was supported by JSPS KAKENHI Grant-in-Aid for Research Activity Start-up (Grant Number 20K22377) and Grant-in-Aid for Early-Career Scientists (Grant Number 23K13490).

References

[1] C.P. Fenimore, F.J. Martin, Flammability of polymers, *Combust. Flame*. 10 (1966) 135–139.

[2] ISO 4589-2, Plastics — Determination of burning behaviour by oxygen index — Part 2: Ambient-temperature test, 2017.

[3] ASTM D2863, Standard Test Method for Measuring the Minimum Oxygen Concentration to Support Candle-Like Combustion of Plastics (Oxygen Index), 2019.

[4] E.D. Weil, N.G. Patel, M.M. Said, M.M. Hirschler, S. Shakir, Oxygen index: Correlations to other fire

tests, *Fire Mater.* 16 (1992) 159–167.

[5] G. Ikeda, Oxygen Index Tests to Evaluate the Suitability of a Given Material for Oxygen Service, in: B.L. Werley (Ed.), Flammbility Sensit. Mater. Oxyg. Atmos. ASTM STP 812, ASTM International, 1983: pp. 56–67.

[6] R.K. Wharton, Correlation between the critical oxygen index test and other fire tests, *Fire Mater.* 5 (1981) 93–102.

[7] E. Orndoff, Investigation of correlations between the oxygen index of polymers and their intrinsic characteristics, Rice University, 1996.

[8] M. SIBULKIN, M. LITTLE, Propagation and extinction of downward burning fires, *Combust. Flame*. 31 (1978) 197–208.

[9] M. Suzanne, M. Delichatsios, J. Zhang, Prediction of the Limiting Oxygen Index Using Simple Flame Extinction Theory and Material Properties Obtained from Bench Scale Measurements, *Fire Saf. Sci.* 10 (2011) 375–387.

[10] M. Suzanne, M.A.A. Delichatsios, J.P.P. Zhang, Flame extinction properties of solids obtained from limiting oxygen index tests, *Combust. Flame*. 161 (2014) 288–294.

[11] S. Bhattacharjee, A. Simsek, F. Miller, S. Olson, P. Ferkul, Radiative, thermal, and kinetic regimes of opposed-flow flame spread: A comparison between experiment and theory, *Proc. Combust. Inst.* 36 (2017) 2963–2969.

[12] O. Fujita, Solid combustion research in microgravity as a basis of fire safety in space, *Proc. Combust. Inst.* 35 (2015) 2487–2502.

[13] K.R. Sacksteder, J.S. Tien, Buoyant downward diffusion flame spread and extinction in partial-gravity accelerations, *Symp. Combust.* 25 (1994) 1685–1692.

[14] S.L. Olson, P. V. Ferkul, J.S. T'ien, Near-limit flame spread over a thin solid fuel in microgravity, *Symp. Combust.* 22 (1989) 1213–1222.

[15] T. Delzeit, L. Carmignani, T. Matsuoka, S. Bhattacharjee, Influence of edge propagation on downward flame spread over three-dimensional PMMA samples, *Proc. Combust. Inst.* 37 (2019) 3203–3209.

[16] X. Huang, S. Link, A. Rodriguez, M. Thomsen, S. Olson, P. Ferkul, C. Fernandez-Pello, Transition from opposed flame spread to fuel regression and blow off: Effect of flow, atmosphere, and microgravity, *Proc. Combust. Inst.* 37 (2019) 4117–4126.

[17] Y. Nakamura, K. Kizawa, S. Mizuguchi, A. Hosogai, K. Wakatsuki, Experimental Study on Near-Limiting Burning Behavior of Thermoplastic Materials with Various Thicknesses Under Candle-Like Burning Configuration, *Fire Technol.* 52 (2016) 1107–1131.

[18] S. Takahashi, H. Ito, Y. Nakamura, O. Fujita, Extinction limits of spreading flames over wires in microgravity, *Combust. Flame*. 160 (2013) 1900–1902.

[19] K. Miyamoto, X. Huang, N. Hashimoto, O. Fujita, C. Fernandez-Pello, Limiting oxygen concentration (LOC) of burning polyethylene insulated wires under external radiation, *Fire Saf. J.* 86 (2016) 32–40.

[20] Y. Konno, N. Hashimoto, O. Fujita, Role of wire core in extinction of opposed flame spread over thin electric wires, *Combust. Flame*. 220 (2020) 7–15.

[21] S. Takahashi, T. Ebisawa, S. Bhattacharjee, T. Ihara, Simplified model for predicting difference between flammability limits of a thin material in normal gravity and microgravity environments, *Proc. Combust. Inst.* 35 (2015) 2535–2543.

[22] S. Takahashi, M.A.F. Bin Borhan, K. Terashima, A. Hosogai, Y. Kobayashi, Flammability limit of thin flame retardant materials in microgravity environments, *Proc. Combust. Inst.* 37 (2019) 4257–4265.

[23] S. Takahashi, K. Terashima, M.A.F. bin Borhan, Y. Kobayashi, Relationship Between Blow-Off Behavior and Limiting Oxygen Concentration in Microgravity Environments of Flame Retardant Materials, *Fire Technol.* 56 (2020) 169–183.

[24] F. Guo, W. Hase, Y. Ozaki, Y. Konno, M. Inatsuki, K. Nishimura, N. Hashimoto, O. Fujita, Experimental study on flammability limits of electrolyte solvents in lithium-ion batteries using a wick combustion method, *Exp. Therm. Fluid Sci.* 109 (2019) 109858.

[25] F. Guo, Y. Ozaki, K. Nishimura, N. Hashimoto, O. Fujita, Influence of lithium salts on the combustion characteristics of dimethyl carbonate-based electrolytes using a wick combustion method, *Combust.*

Flame. 213 (2020) 314–321.

[26] F. Guo, Y. Ozaki, K. Nishimura, N. Hashimoto, O. Fujita, Experimental study on flame stability limits of lithium ion battery electrolyte solvents with organophosphorus compounds addition using a candle-like wick combustion system, *Combust. Flame*. 207 (2019) 63–70.

[27] F. Guo, Y. Ozaki, Y. Konno, N. Hashimoto, O. Fujita, Near-limit oscillatory behaviors on wick flames of dimethyl carbonate with trimethyl phosphate additions, *Proc. Combust. Inst.* 38 (2021) 4691–4698.

[28] S. Bhattacharjee, L. Carmignani, Radiation-kinetics interactions: A comparison of opposed-flow flame spread in a low-velocity microgravity and low-pressure downward environments, *Proc. Combust. Inst.* 38 (2021) 4795–4803.

[29] S. Bhattacharjee, K. Dong, A numerical investigation of radiation feedback in different regimes of opposed flow flame spread, *Int. J. Heat Mass Transf.* 150 (2020) 119358.

[30] A.C. Fernandez-Pello, S.R. Ray, I. Glassman, Flame spread in an opposed forced flow: the effect of ambient oxygen concentration, *Symp. Combust.* 18 (1981) 579–589.

[31] A.C. Fernandez-Pello, T. HIRANO, Controlling Mechanisms of Flame Spread, *Combust. Sci. Technol.* 32 (1983) 1–31.

[32] S.H. Chung, Stabilization, propagation and instability of tribrachial triple flames, *Proc. Combust. Inst.* 31 (2007) 877–892.

[33] C.K. Law, Combustion Physics, Cambridge University Press, Cambridge, 2006.

[34] M. Matalon, Flame dynamics, *Proc. Combust. Inst.* 32 (2009) 57–82.

[35] Y.-X. Tao, M. Kaviany, Burning rate of liquid supplied through a wick, *Combust. Flame*. 86 (1991) 47–61.

[36] C.-H. Chen, F.-B. Weng, Flame Stabilization and Blowoff Over a Porous Cylinder, *Combust. Sci. Technol.* 73 (1990) 427–446.

[37] H.-Y. Lyu, L.-D. Chen, Numerical modeling of buoyant ethanol-air wick diffusion flames, *Combust. Flame*. 87 (1991) 169–181.

[38] M.P. Raju, J.S. T'ien, Modelling of candle burning with a self-trimmed wick, *Combust. Theory Model.*

12 (2008) 367–388.

[39] F.J. Kosdon, F.A. Williams, C. Buman, Combustion of vertical cellulosic cylinders in air, *Symp. Combust.* 12 (1969) 253–264.

[40] S.H. Wu, L.-D. Chen, Numerical simulation of wick diffusion flames, *J. Propuls. Power*. 8 (1992) 921–926.

[41] N. Riley, A sheet model for the candle flame, *R. Soc.* 442 (1993) 361–372. http://rspa.royalsocietypublishing.org/content/442/1915/361.short.

[42] D.L. Dietrich, H.D. Ross, Y. Shu, P. Chang, J.S. T'ien, Candle Flames in Non-Buoyant Atmospheres, *Combust. Sci. Technol.* 156 (2000) 1–24.

[43] A. Alsairafi, S.-T. Lee, J.S. T'ien, Modeling gravity effect on diffusion flames stabilized around a cylindrical wick saturated with liquid fuel, *Combust. Sci. Technol.* 176 (2004) 2165–2191.

[44] A. Kumar, H.Y. Shih, J.S. T'ien, A comparison of extinction limits and spreading rates in opposed and concurrent spreading flames over thin solids, *Combust. Flame*. 132 (2003) 667–677.

[45] A. Kumar, J.S. T'ien, Numerical Modeling of Limiting Oxygen Index Apparatus for Film Type Fuels, *Int. J. Spray Combust. Dyn.* 4 (2012) 299–322.

[46] A. Kumar, K. Tolejko, J.S. T'ien, A Computational Study on Flame-Solid Radiative Interaction in Flame Spread Over Thin Solid-Fuel, *J. Heat Transfer*. 126 (2004) 611.

[47] A. Kumar, J. Tien, A computational study of low oxygen flammability limit for thick solid slabs, *Combust. Flame*. 146 (2006) 366–378.

[48] NuFD, FrontFlow/Red, (2005). www.ciss.iis.u-tokyo.ac.jp/fsis/en/ (accessed December 12, 2022).

[49] M.D. Smooke, V. Giovangigli, Formulation of the premixed and nonpremixed test problems, in: M.D. Smooke (Ed.), Reduc. Kinet. Mech. Asymptot. Approx. Methane-Air Flames., Springer Berlin, Heidelberg, 1991: pp. 1–28.

[50] T.L. Bergman, F.P. Incropera, D.P. Dewitt, A.S. Lavine, Fundamentals of Heat and Mass Transfer, 5th Edition, John Wiley & Sons., 2011.

[51] N. Hashimoto, R. Kurose, S.-M. Hwang, H. Tsuji, H. Shirai, A numerical simulation of pulverized

coal combustion employing a tabulated-devolatilization-process model (TDP model), *Combust. Flame*. 159 (2012) 353–366.

[52] N. Hashimoto, R. Kurose, H. Shirai, Numerical simulation of pulverized coal jet flame employing the TDP model, *Fuel*. 97 (2012) 277–287.

[53] C.K. Westbrook, F.L. Dryer, Simplified Reaction Mechanisms for the Oxidation of Hydrocarbon Fuels in Flames, *Combust. Sci. Technol.* 27 (1981) 31–43.

[54] Reaction Design, CHEMKIN-PRO, 2013.

[55] A. Mishra, P. Sharma, M. Kumar, A. Ray, Flame structure and stability for oxygen enhanced non-premixed combustion of highly diluted methane with helium and nitrogen, *Fuel*. 347 (2023) 128469.

[56] P. Sunderland, B. Mendelson, Z. Yuan, D. Urban, Shapes of buoyant and nonbuoyant laminar jet diffusion flames, *Combust. Flame*. 116 (1999) 376–386.

[57] F. Takahashi, V.R. Katta, A reaction kernel hypothesis for the stability limit of methane jet diffusion flames, *Proc. Combust. Inst.* 28 (2000) 2071–2078.

[58] S.H. Won, J. Kim, K.J. Hong, M.S. Cha, S.H. Chung, Stabilization mechanism of lifted flame edge in the near field of coflow jets for diluted methane, *Proc. Combust. Inst.* 30 (2005) 339–347.

[59] F. Takahashi, V.R. Katta, Structure of propagating edge diffusion flames in hydrocarbon fuel jets, *Proc. Combust. Inst.* 30 (2005) 375–382.

[60] M.K. Kim, S.H. Won, S.H. Chung, Effect of velocity gradient on propagation speed of tribrachial flames in laminar coflow jets, *Proc. Combust. Inst.* 31 (2007) 901–908.

[61] G.R. Ruetsch, L. Vervisch, A. Liñán, Effects of heat release on triple flames, *Phys. Fluids*. 7 (1995) 1447–1454.

[62] S. Ghosal, L. Vervisch, Theoretical and numerical study of a symmetrical triple flame using the parabolic flame path approximation, *J. Fluid Mech.* 415 (2000) 227–260.

[63] N.M. Marinov, A detailed chemical kinetic model for high temperature ethanol oxidation, *Int. J. Chem. Kinet.* 31 (1999) 183–220.

[64] “Chemical-Kinetic Mechanisms for Combustion Applications”, San Diego Mechanism web page,

Mechanical and Aerospace Engineering (Combustion Research), University of California at San Diego, (n.d.). http://combustion.ucsd.edu (accessed November 15, 2022).

[65] A.A. Konnov, R.J. Meuwissen, L.P.H. de Goey, The temperature dependence of the laminar burning velocity of ethanol flames, *Proc. Combust. Inst.* 33 (2011) 1011–1019.

[66] F.N. Egolfopoulos, D.X. Du, C.K. Law, A study on ethanol oxidation kinetics in laminar premixed flames, flow reactors, and shock tubes, *Symp. Combust.* 24 (1992) 833–841.

[67] D. Bradley, M. Lawes, M.S. Mansour, Explosion bomb measurements of ethanol–air laminar gaseous flame characteristics at pressures up to 1.4MPa, *Combust. Flame*. 156 (2009) 1462–1470.

[68] Ö.L. Gülder, Laminar burning velocities of methanol, ethanol and isooctane-air mixtures, *Symp. Combust.* 19 (1982) 275–281.